Statistical characterization of weak scattering fields with inverse methods

Angeliki Xenaki*, Peter Gerstoft†, Olivier Carriere† and Klaus Mosegaard*
*Department of Applied Mathematics and Computer Science, Technical University of Denmark, 2800 Kgs. Lyngby, Denmark
†Scripps Institution of Oceanography, University of California San Diego, La Jolla, CA 92093-0238, USA

***Abstract*—In an acoustic backscattering model of a stationary field of volume inhomogeneities, a stochastic description of the field is more useful than a deterministic description due to the complex nature of the field. A method based on linear inversion is employed to infer information about the statistical properties of the scattering field from the obtained cross-spectral matrix.**

I. Introduction

Determination of the statistical properties of volume reverberation is crucial for dictating the level of false alarm in the design of detection methods [1], [2] and for correlating the acoustic return to the characteristics of known sediments in remote sediment classification [3]–[5]. Hence, substantial effort has been focused on modeling weak scattering [6]–[9]. High-frequency active sonars provide high-resolution measurements and improve volume backscattering models by means of detection of small scale structure as individual scatterers play a more important role in determining scattering parameters [1]–[5]. Typically, volume reverberation is described by the statistical distribution of the backscattering strength, which is defined as the ratio of the scattered intensity to the incident intensity per unit volume in dB [3], [10]–[13].

The backscattering strength is proportional to the cross spectral density of the scattering field thus related to its statistical properties such as variance and correlation lengths [1], [5], [14]. However, for narrowband measurements the backscattering strength provides a single measure and additional information for covariance parameters are required to relate the spatial variation of the scattering field to a covariance function.

Herein, the weak scattering approach is applied for studying the backscattering from inhomogeneous substances in the water column and specifically for the characterization of submerged oil from a deep-water oil leak. In such cases, there are indications that a significant quantity of oil remains submerged and extends throughout the water column as elongated formations of viscous material mixed with water and possibly with biological material [15], [16]. Since the existence of submerged oil is controlled by the ambient density, the difference in the acoustic parameters between the two fluid media is small producing weak scattering of the incident acoustic energy [3], [13]. The submerged oil in the water is modeled as a fluid medium exhibiting spatial heterogeneity. A random field generator [17] is used to implement a physical model of the inhomogeneous medium and a high-frequency active sonar is selected to collect the backscattered returns.

A new method is developed which allows to describe volume scattering models quantitatively in terms of their statistical properties. Determining the correlation function of the field parameters directly with inverse methods gives a better measure of the volume reverberation statistical characteristics.

The theory of Toeplitz matrices [18] is employed to study the stability of the solution and thus the quality of the reconstruction.

II. Forward problem

A. Scattering from inhomogeneities

The scattered sound pressure p_s observed at a remote position $\mathbf{r}_0$ due to scattering from spatial fluctuations of the compressibility $\epsilon_\kappa(\mathbf{r})$ and density $\epsilon_\rho(\mathbf{r})$ of the medium within a scattering region R (see Fig. 1) is given by the integral equation [19],

$$p_s(\mathbf{r}_0) = \int_R \left(k^2 \epsilon_\kappa(\mathbf{r}) p(\mathbf{r}) - \nabla\,[\epsilon_\rho(\mathbf{r}) \nabla\, p(\mathbf{r})]\right) g(\mathbf{r}_0|\mathbf{r})\,\mathrm{d}\mathbf{r}, \quad (1)$$

where k is the wavenumber, $p(\mathbf{r})$ is the wave insonifying the scatterer located at $\mathbf{r}$ and $g(\mathbf{r}_0|\mathbf{r}) = \frac{1}{4\pi|\mathbf{r}_0-\mathbf{r}|} e^{-ik|\mathbf{r}_0-\mathbf{r}|}$ is the free-space Green's function which describes the sound pressure at an observation point $\mathbf{r}_0$ due to a point source at $\mathbf{r}$. The harmonic time dependence $e^{i\omega t}$ is implied and neglected for simplicity. The compressibility and density fluctuations are normalized to their mean values, $\epsilon_\kappa(\mathbf{r}) = \frac{\delta\kappa(\mathbf{r})}{\langle\kappa\rangle}$, $\epsilon_\rho(\mathbf{r}) = \frac{\delta\rho(\mathbf{r})}{\langle\rho\rangle}$, thus are dimensionless quantities with zero mean value, $\langle\epsilon_\kappa(\mathbf{r})\rangle = 0$ and $\langle\epsilon_\rho(\mathbf{r})\rangle = 0$.

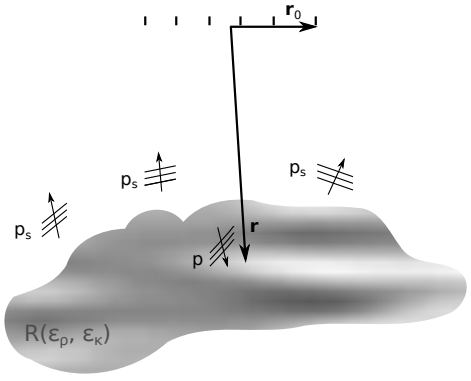

Fig. 1. Schematic for backscattering from an inhomogeneous field R.

For far field radiation, the Fraunhofer approximation for the range term is valid [20],

$$|\mathbf{r}_0 - \mathbf{r}| \approx r - \hat{\mathbf{r}} \cdot \mathbf{r}_0, \tag{2}$$

where $r = |\mathbf{r}|$ and $\hat{\mathbf{r}} = \frac{\mathbf{r}}{r}$ is the unit vector in the direction of $\mathbf{r}$ and the Green's function takes the simpler form,

$$g(\mathbf{r}_0|\mathbf{r}) \approx \frac{1}{4\pi r} e^{-ik(r - \hat{\mathbf{r}}\cdot\mathbf{r}_0)}. \tag{3}$$

The incident wave which insonifies the region R emanates from a monopole located at the origin of the coordinate system out of the scattering region R,

$$p_i(\mathbf{r}) = A\frac{e^{-ikr}}{r}, \tag{4}$$

where A is the pressure amplitude at a distance 1 m from the source and r denotes the range of the insonified point.

Assuming weak scattering, the Born approximation applies, $p \approx p_i$. Thus, inserting Eqs. (3) and (4) in Eq. (1) the pressure scattered from inhomogeneities in the acoustic parameters of the medium is,

$$p_s(\mathbf{r}_0) \approx \frac{k^2 A}{4\pi} \int\limits_R \left([\epsilon_\kappa(\mathbf{r}) - \epsilon_\rho(\mathbf{r})] \frac{e^{-ik(2r - \hat{\mathbf{r}}\cdot\mathbf{r}_0)}}{r^2} \right) \mathrm{d}\mathbf{r}. \tag{5}$$

The density fluctuations are neglected henceforth since they are proportional to the compressibility fluctuations and are less significant in fluid media [11], [21].

Owing to the Born approximation, Eq. (5) relates linearly the backscattered pressure and the fluctuations in the acoustic parameters and can be discretized and rearranged in a matrix-vector formulation.

B. Discretization of the propagation model

An active sonar in a monostatic configuration (the transmitter and receiver array are collocated) is assumed. The transmitter emits a narrowband high-frequency pulse and is supposed to have a narrow directivity pattern in the along-track plane, thus the monochromatic case is considered and only the 2D across-track plane is modeled. The receiver comprises sensors arranged in a uniform linear array centered at the origin of the coordinate system such that the sensors locations are $x_q = (q - \frac{N_s+1}{2})d_s$, $q = 1, 2, \cdots, N_s$, where N_s is the number of sensors with interelment spacing d_s. Hence $\hat{\mathbf{r}_j} \cdot \mathbf{r}_0 = x_q \sin(\theta_j)$ in Eq. (2), where θ_j is the angle between the z-axis and the j^{th} scatterer.

For reasons that will become apparent in the following, the model parameters are discretized on a 2D grid equidistantly spaced in $\sin(\theta)$ and r. To simplify the notation, the variable $u = \sin(\theta)$ is introduced such that $\hat{\mathbf{r}_j} \cdot \mathbf{r}_0 = x_i u_j$.

Dynamic focusing is used to relate the focusing distance with the arrival time [20], [22]. The scattered pressure at the sensor located at x_q at the focusing range r_l is,

$$p_s(x_q, r_l) = \frac{k^2 A}{4\pi} \frac{e^{-ik2r_l}}{r_l^2} \mathrm{d}r \sum_j^{N_u} \epsilon_\kappa(u_j, r_l) e^{ikx_q u_j} r_l \mathrm{d}u. \tag{6}$$

The forward problem can be written in a matrix formulation,

$$\mathbf{d} = \mathbf{G}\mathbf{m} + \mathbf{n}, \tag{7}$$

where $\mathbf{d}$ is the $N \times 1$ vector comprising the acquired data (the scattered returns possibly contaminated with additive noise described by the $N \times 1$ vector $\mathbf{n}$), $\mathbf{G}$ is the $N \times M$ linear forward matrix and $\mathbf{m}$ is the $M \times 1$ vector of model parameters, namely the compressibility fluctuations.

More analytically, Table I shows the model parameters arranged on the 2D grid, where N_u is the number of arrival directions and N_r is the number of focusing depths. The total number of model parameters is $M = N_r N_u$.

TABLE I. MODEL GRID.

m_1	m_2	$\cdots$	m_{N_u}
m_{N_u+1}	m_{N_u+2}	$\cdots$	m_{2N_u}
$\vdots$	$\vdots$	$\ddots$	$\vdots$
$m_{(N_r-1)N_u+1}$	$m_{(N_r-1)N_u+2}$	$\cdots$	$m_{N_r N_u}$

The vector $\mathbf{m}$ of the model parameters is formed by stacking the rows of the model grid,

$$\mathbf{m}_{M\times 1} = \begin{bmatrix} \epsilon_\kappa(u_1, r_1) \\ \vdots \\ \epsilon_\kappa(u_{N_u}, r_1) \\ \epsilon_\kappa(u_1, r_2) \\ \vdots \\ \epsilon_\kappa(u_{N_u}, r_2) \\ \vdots \\ \epsilon_\kappa(u_1, r_{N_r}) \\ \vdots \\ \epsilon_\kappa(u_{N_u}, r_{N_r}) \end{bmatrix} = \begin{bmatrix} m_1 \\ \vdots \\ m_{N_u} \\ m_{N_u+1} \\ \vdots \\ m_{2N_u} \\ \vdots \\ m_{(N_r-1)N_u+1} \\ \vdots \\ m_{N_r N_u} \end{bmatrix}. \tag{8}$$

The data vector comprises the scattered pressure at each sensor x_q, $q = 1, 2, \cdots, N_s$ at each focusing range r_l, $l = 1, 2, \cdots, N_r$ (total number of elements $N = N_s N_r$) and additive noise,

$$\mathbf{d}_{N\times 1} = \begin{bmatrix} d_1 \\ d_2 \\ \vdots \\ d_N \end{bmatrix} = \begin{bmatrix} p_s(x_1, r_1) \\ \vdots \\ p_s(x_{N_s}, r_1) \\ p_s(x_1, r_2) \\ \vdots \\ p_s(x_{N_s}, r_2) \\ \vdots \\ p_s(x_1, r_{N_r}) \\ \vdots \\ p_s(x_{N_s}, r_{N_r}) \end{bmatrix} + \begin{bmatrix} n_1 \\ n_2 \\ \vdots \\ n_N \end{bmatrix}. \quad (9)$$

The noise is assumed to be complex Gaussian with zero mean and covariance matrix $\mathbf{C}_n$ such that $\mathbf{n} \sim CN(0, \mathbf{C}_n)$. The noise covariance matrix is diagonal with the diagonal elements equal to the standard deviation σ_n.

Due to dynamic focusing, the forward matrix has a range-dependent structure,

$$\mathbf{G}(r_l)_{N_s\times N_u} \propto \frac{e^{-ik2r_l}}{r_l} \begin{bmatrix} e^{ikx_1u_1} & \dots & e^{ikx_1u_{N_u}} \\ e^{ikx_2u_1} & \dots & e^{ikx_2u_{N_u}} \\ \vdots & \ddots & \vdots \\ e^{ikx_{N_s}u_1} & \dots & e^{ikx_{N_s}u_{N_u}} \end{bmatrix}. \quad (10)$$

The matrix $\mathbf{G}(r_l)$ contains the propagation phase shifts between all N_s sensors on the ULA positioned at x_q, $q = 1, 2, \cdots, N_s$ and all N_u arrival directions u_j, $j = 1, 2, \cdots N_u$ at the focusing distance r_l.

The total $\mathbf{G}_{N\times M}$ matrix where $N = N_sN_r$, $M = N_uN_r$, is a block matrix which is constructed by the direct sum of $\mathbf{G}(r_l)$ for $l = 1, 2, \cdots N_r$.

$$\mathbf{G}_{N\times M} = \begin{bmatrix} \mathbf{G}(r_1) & \mathbf{0} & \cdots & \mathbf{0} \\ \mathbf{0} & \mathbf{G}(r_2) & \cdots & \mathbf{0} \\ \vdots & \vdots & \ddots & \vdots \\ \mathbf{0} & \mathbf{0} & \cdots & \mathbf{G}(r_{N_r}) \end{bmatrix}. \quad (11)$$

III. Inverse problem

Assuming that the random field of model parameters is stationary, the model covariance matrix, $\mathbf{C}_m$, has a Toeplitz structure determined by the covariance function. As the model parameters which are more than a characteristic length (defined as the lag distance where the covariance function has decayed by 95%) apart are practically uncorrelated, the dimensions of the problem is significantly reduced [23] when the interest is in solving for the model covariance function and not for the model parameters *per se*.

The forward linear problem (Eq. (7)) yields,

$$\begin{aligned} \mathbf{dd}^H &= (\mathbf{Gm} + \mathbf{n}) \left(\mathbf{m}^T\mathbf{G}^H + \mathbf{n}^H \right) \\ &= \mathbf{Gmm}^T\mathbf{G}^H + \mathbf{Gmn}^H + \mathbf{nm}^T\mathbf{G}^H + \mathbf{nn}^H, \end{aligned} \quad (12)$$

where the symbol ^{T} denotes transpose and the symbol ^{H} denotes conjugate transpose of a vector or matrix. Considering the ensemble average and assuming that the noise is uncorrelated with the model parameters, Eq. (12) yields,

$$< \mathbf{dd}^H >= \mathbf{G} < \mathbf{mm}^T > \mathbf{G}^H + < \mathbf{nn}^H > . \quad (13)$$

Thus, the data covariance matrix $\mathbf{C}_d =< \mathbf{dd}^H >$, and the model covariance matrix $\mathbf{C}_m =< \mathbf{mm}^T >$ are connected through the relation,

$$\mathbf{C}_d = \mathbf{GC}_m\mathbf{G}^H + \mathbf{C}_n \quad (14)$$

where $\mathbf{C}_n =< \mathbf{nn}^H >$ is the covariance matrix of the noise.

Inversion of Eq. (14) with the least-squares approach yields,

$$\hat{\mathbf{C}}_m = \mathbf{G}^+\mathbf{C}_d \left(\mathbf{G}^+\right)^H, \quad (15)$$

where $^+$ denotes generalized inverse.

Herein we are concerned with the overdetermined problem, that is $N > M$.

IV. Eigenvalue structure of the forward operator

The stability of the solution (Eq. (15)) is examined through the singular values of the matrix $\mathbf{G}$. Since the singular values of a block matrix are the combined singular values of its blocks, it is sufficient to examine the singular value structure of $\mathbf{G}(r_l)$. In the overdetrmined case, where $N > M$ and thus according to Eq. (11) $N_s > N_u$, the singular values of $\mathbf{G}(r_l)$ are the square roots of the eigenvalues of $\mathbf{G}^H(r_l)\mathbf{G}(r_l)$.

The matrix $\mathbf{G}^H(r_l)\mathbf{G}(r_l)$ is Hermitian Toeplitz for equidistant spacing in u, such that $u_i - u_j = d_u(i - j)$, $i, j = 1, 2, \cdots, N_u$; see Eq. (16).

Since the Toeplitz matrix of concern is Hermitian, it is completely specified by the elements on the first row. The elements on the first row are samples from the periodic sinc function,

$$\mathbf{G}^H(r_l)\mathbf{G}(r_l)_{N_u\times N_u} \propto \frac{1}{r_l^2}\begin{bmatrix} N_s & \sum_{q=1}^{N_s} e^{-ikx_q(u_1-u_2)} & \dots & \sum_{q=1}^{N_s} e^{-ikx_q(u_1-u_{N_u})} \\ \sum_{q=1}^{N_s} e^{-ikx_q(u_2-u_1)} & N_s & \dots & \sum_{q=1}^{N_s} e^{-ikx_q(u_2-u_{N_u})} \\ \vdots & \vdots & \vdots & \vdots \\ \sum_{q=1}^{N_s} e^{-ikx_q(u_{N_u}-u_1)} & \sum_{q=1}^{N_s} e^{-ikx_q(u_{N_u}-u_2)} & \dots & N_s \end{bmatrix} \tag{16}$$

$$\begin{aligned} f(u) &= \sum_{q=1}^{N_s} e^{-ikx_q u} \\ &= \sum_{q=1}^{N_s} e^{-i2\pi\frac{d_s}{\lambda}\left(i-\frac{N_s-1}{2}\right)u} \\ &= e^{-i2\pi\frac{d_s}{\lambda}\left(\frac{1-N_s}{2}\right)u}\sum_{q=1}^{N_s} e^{-i2\pi\frac{d_s}{\lambda}(i-1)u} \\ &= e^{-i2\pi\frac{d_s}{\lambda}\left(\frac{1-N_s}{2}\right)u}\frac{1-e^{-i\pi N_s\frac{d_s}{\lambda}u}}{1-e^{-i2\pi\frac{d_s}{\lambda}u}} \\ &= e^{-i2\pi\frac{d_s}{\lambda}\left(\frac{1-N_s}{2}\right)u}\frac{e^{-i\pi N_s\frac{d_s}{\lambda}u}2i\sin\left(\pi N_s\frac{d_s}{\lambda}u\right)}{e^{-i\pi\frac{d_s}{\lambda}u}2i\sin\left(\pi\frac{d_s}{\lambda}u\right)} \\ &= \frac{\sin\left(\pi N_s\frac{d_s}{\lambda}u\right)}{\sin\left(\pi\frac{d_s}{\lambda}u\right)}. \end{aligned} \tag{17}$$

The generating function $f(u)$ is the discrete Fourier transform of the rectangle function $\Pi\left(\frac{x}{W}\right)$ with unit height and base width $W = \frac{L_s}{\lambda}$, where $L_s = N_s d_s$ is the length of the array, sampled at N_s points with spacing d_s and can be recognised as the beampattern as a function of u. As shown in Fig. 2, the zeros of the function occur at $u = q\frac{\lambda}{N_s d_s}$ for $q \in \{\mathbb{Z} - pN_s\}$ and $p \in \mathbb{Z}$. The function is bounded by the maximum arrival direction considered in the visible region $u_{max} \leq 1$. In order to avoid aliasing, the condition $\frac{\lambda}{2d_s} > u_{max}$ should be fulfilled.

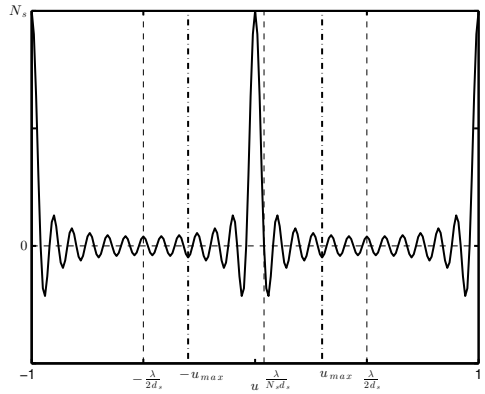

Fig. 2. The sinc periodic function $\frac{\sin(\pi\frac{N_s d_s}{\lambda}u)}{\sin(\pi\frac{d_s}{\lambda}u)}$ as a function of u.

Hence, the elements of the matrix $\mathbf{G}^H(r_l)\mathbf{G}(r_l)$ are,

$$\left[\mathbf{G}^H(r_l)\mathbf{G}(r_l)\right]_{ij} \propto \frac{1}{r_l^2}\frac{\sin(\pi\frac{N_s d_s}{\lambda}d_u|i-j|)}{\sin(\pi\frac{d_s}{\lambda}d_u|i-j|)} \tag{18}$$

The eigenvalue structure of Toeplitz matrices can be deduced by relating the properties of Toeplitz matrices to those of their simpler special case, the circulant matrices. These two types of matrices are equivalent in an asymptotic sense and this is shown to imply that their eigenvalues among other characteristics behave similarly. The eigenvalues of circulant matrices can be found exactly as the Fourier transform of the elements in the first row [18], [24]. Since u is bounded, $|u| \leq u_{max} \leq 1$, the corresponding Toeplitz matrix is of finite order and is shown in [24] that asymptotically its eigenvalues are samples of the Fourier spectrum of the series connected with the Toeplitz structure.

Assuming $\frac{\lambda}{2d_s} > u_{max}$ the eigenvalues are determined by the sampling of the Fourier transform of the truncated sinc function (Fig. 3). Denoting $W = \frac{N_s d_s}{\lambda}$, in case of oversampling when $d_u < \frac{1}{W}$ there will be zero eigenvalues and the matrix $\mathbf{G}^H\mathbf{G}$ will be rank deficient [25]. Otherwise, when $d_u \geq \frac{1}{W}$, the matrix $\mathbf{G}^H\mathbf{G}$ is full rank.

Figure 3 shows the effect of the grid spacing d_u on the eigenvalues of the matrix $\mathbf{G}^H\mathbf{G}$ for fixed frequency and receiving array configuration. The higher the frequency and/or the longer the receiving array, the finer the resolution that can be achieved in terms of d_u. Note that fewer sensors can be used with larger interelement spacing without altering the total length of the array as long as the condition $\frac{\lambda}{2d_s} > u_{max}$ is satisfied.

Naturally, the field of model parameters exhibits stationarity in the Cartesian coordinate system, which implies that it is not stationary in the spherical coordinate system. However, confining the insonified area within an opening angle $[-15°, 15°]$ the curvature is negligible and $d_u \approx d_\theta \approx \frac{d_x}{r}$ and $d_r \approx d_z$. The longer the focusing distance, the coarser the resolution, in terms of d_x.

A. Regularization by truncated SVD

In case of oversampling, $d_u < \frac{N_s d_s}{\lambda}$, the matrix $\mathbf{G}^H\mathbf{G}$ will have zero eigenvalues and regularization needs to be applied. Due to the specific structure of eigenvalues (Fig. 3 (c)), the truncated SVD method is chosen. The truncation parameter is chosen as the width $d_u W$ of the rectangle function.

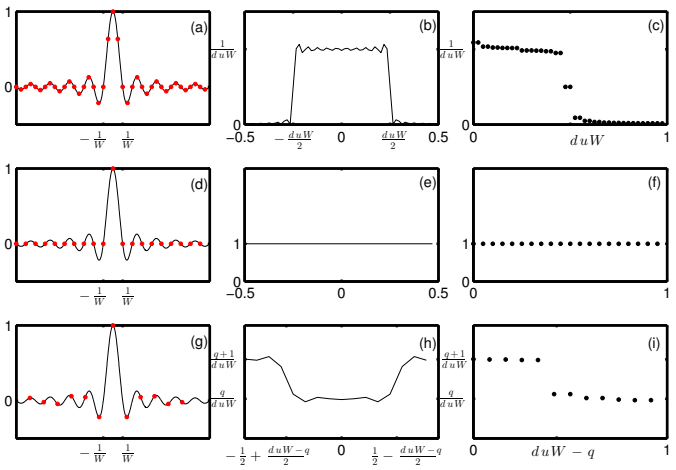

Fig. 3. (a), (d), (g) Sampled truncated sinc function, (b), (e), (h) the corresponding spectrum and (c), (f), (i) the corresponding eigenvalue spectrum. Effect of the sampling distance d_u on the eigenvalues of the matrix $\mathbf{G}^H\mathbf{G}$ for fixed W (frequency and array configuration). (a)-(c) Oversampling $d_u < \frac{1}{W}$, (d)-(f) critical sampling $d_u = \frac{1}{W}$ and (g)-(i) undersampling $d_u > \frac{1}{W}$, $\{q \in \mathbb{N} |\ q < Wdu < q+1\}$.

V. Simulation Results

A synthetic example is build to demonstrate the method. A uniform linear array is considered comprising $N_s = 256$ sensors with interelement spacing $d_s = 1.6$ mm. The field is insonified by a narrowband 200 kHz source. The duration of the pulse is 120 μs corresponding to a range resolution of 0.1 m ($c = 1500$ m/s) [26].

A 2D field of compressibility fluctuations is considered, representing a region of oil contamination within the water column. The contaminated region is expected to have higher viscosity than the surrounding seawater and present layering due to interface tension [27]. The field is assumed stationary with a constant mean value characterized by an anisotropic Gaussian covariance function with variance $\sigma_\kappa^2 = 0.01$ and correlation lengths 2 m in x-direction and 0.5 m in z-direction [28]. The variance is the value of the covariance function at zero lag and the correlation lengths are the lag distances where the covariance function has decayed by at least 95%.

An area of $x = [-4.5 : 1 : 4.5]$ m and $z = [55 : 0.1 : 55.9]$ m is considered. The data covariance matrix is calculated from an ensemble average from 500 pings and additive Gaussian noise is assumed $n \sim \mathcal{CN}(0, 0.01)$. Figure 4 shows the actual model covariance matrix and the result of the least-square inversion. Since the field of model parameters is spatially stationary, the model covariance matrix is symmetric block Toeplitz with the covariance function as the generating function. Thus the covariance function can be deduced from the elements in the first row of the covariance matrix. In order to improve the estimate, the covariance function is calculated by averaging the elements across the blocks in the diagonals and across the diagonals in each block of the covariance matrix.

Due to the ordering of the model parameters on the model vector, the first N_u elements of the covariance function are related to the covariance in u-dimension while the elements $[1 : N_u : M]$ are related to the covariance in r-dimension.

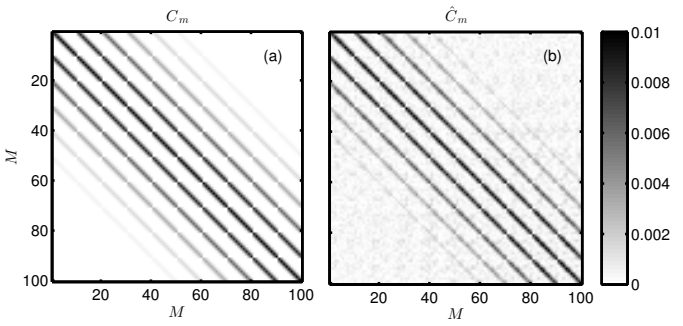

Fig. 4. (a) True and (b) reconstructed model covariance matrix.

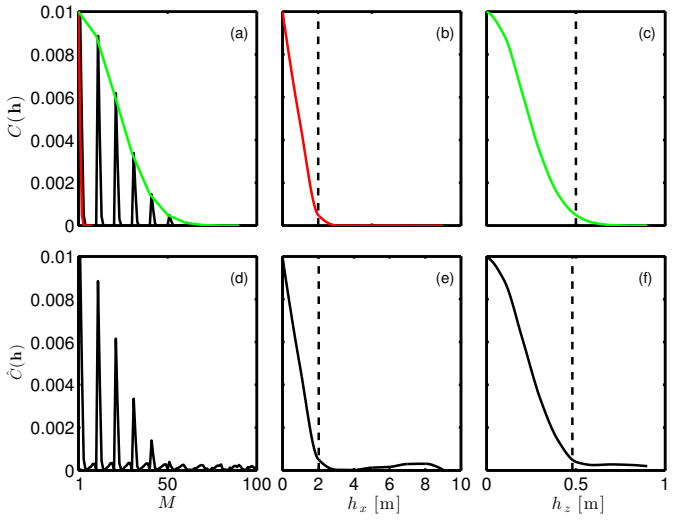

Fig. 5. (a)-(c) True and (d)-(f) reconstructed model covariance function as a function of the lag-distance h_x ((b), (e)) and h_z ((c), (f)) in x and z-direction respectively. The characteristic lengths are denoted by dashed lines in each case.

Since $d_u \approx \frac{d_x}{r}$ and $d_r \approx d_z$, the covariance can be expressed in the x and z-direction as a function of the lag distances $h_x = (0 : N_u - 1)d_u r$ and $h_z = (0 : N_r - 1)d_r$ respectively.

Figure 5 shows the true and reconstructed covariance function and the characteristic lengths.

A. Effect of the number of pings

Figure 6 shows the estimates for the variance, the characteristic length in the x-direction and the characteristic length in z-direction in relation to the number of pings. All the estimates have converged to their true values after averaging over 300 pings.

B. Effect of the regularization by truncated SVD

Figure 7 shows the estimates for the variance, the characteristic length in the x-direction and the characteristic length in z-direction in relation to the ratio of significant eigenvalues to the total number of eigenvalues corresponding to a decrease in the sampling distance d_u.

VI. Conclusion

For stationary scattering fields the method of covariance inference allows significant reduction of the dimensions of the

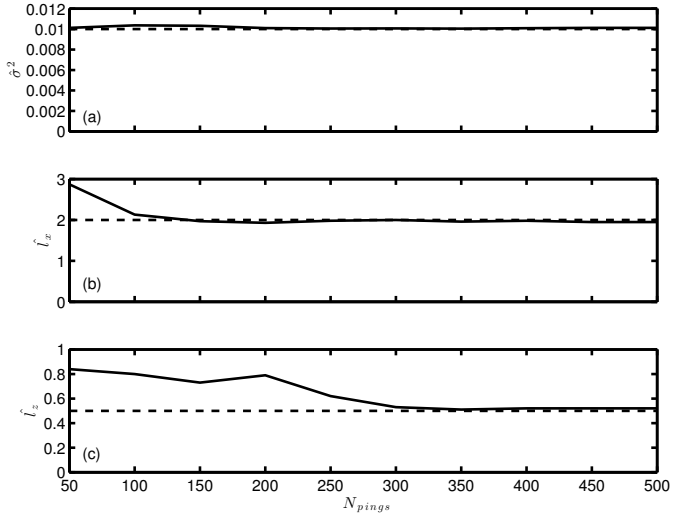

Fig. 6. Estimates as a function of averaging over a number of pings. (a) variance, (b) characteristic length in x-direction, (c) characteristic length in z-direction. The dashed lines denote the true value in each case.

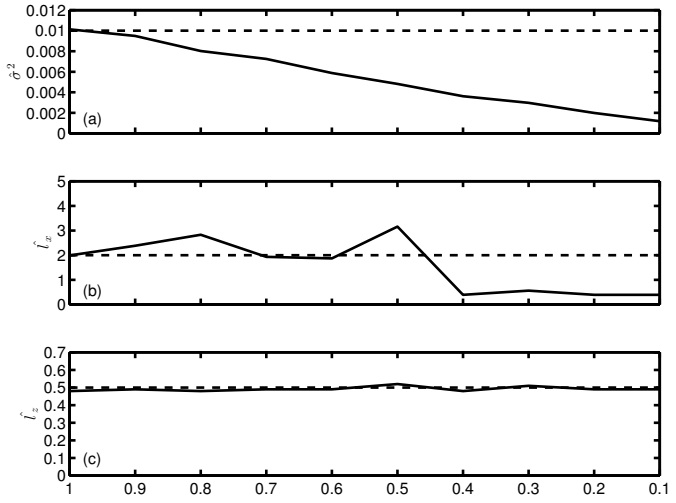

Fig. 7. TSVD estimates. (a) variance, (b) characteristic length in x-direction, (c) characteristic length in z-direction. The dashed lines denote the true value in each case.

problem. Generally, in a medium where there is flow as in the water column, the scattering field will not be static so a deterministic description has less to offer. Localization of the contaminated region can be provided by beamforming and identification by inference of the covariance characteristics of the model covariance.

ACKNOWLEDGMENT

This work has been supported by the Danish National Advanced Technology Foundation, Otto Moensteds Fond, Julie von Müllens Fond, Niels Bohr Fond and Oticon Fond.

REFERENCES

[1] A. A. Douglas and A. P. Lyons, "Novel physical interpretations of K-distributed reverberation," *IEEE J. Oceanic Eng.*, vol. **27**, no. 4, pp. 800–813, 2002.

[2] A. P. Lyons and A. A. Douglas, "Statistical characterization of high-frequency shallow-water seafloor backscatter," *J. Acoust. Soc. Am.*, vol. **106**, no. 1, pp. 1307–1315, 1999.

[3] L. R. LeBlanc, S. G. Schock, D. D. L., M. Jenkins, and L. Munro, "High-resolution sonar volume scattering measurements in marine sediments," *J. Acoust. Soc. Am.*, vol. **97**, no. 5, pp. 2979–2986, 1995.

[4] D. R. Jackson, K. B. Briggs, and M. D. Richardson, "Tests of models for high-frequency seafloor backscatter," *IEEE J. Oceanic Eng.*, vol. **21**, no. 4, pp. 458–470, 1996.

[5] A. N. Gavrilov and I. M. Parnum, "Fluctuations of seafloor backscatter data from multibeam sonar systems," *IEEE J. Oceanic Eng.*, vol. **35**, no. 2, pp. 209–219, 2010.

[6] P. Hines, "Theoretical model of acoustic backscatter from a smooth seabed," *J. Acoust. Soc. Am.*, vol. **88**, pp. 324–334, 1990.

[7] T. Yamamoto, "Acoustic scattering in the ocean from velocity and density fluctuations in the sediments," *J. Acoust. Soc. Am.*, vol. **99**, no. 2, pp. 866–879, 1996.

[8] K. LePage and H. Schmidt, "Spectral integral representations of monostatic backscattering from three-dimensional distributions of sediment volume inhomogeneities," *J. Acoust. Soc. Am.*, vol. **113**, no. 2, pp. 789–799, 2003.

[9] A. Turgut, "Inversion of bottom/subbottom statistical parameters from acoustic backscatter data," *J. Acoust. Soc. Am.*, vol. **102**, no. 2, pp. 833–852, 1997.

[10] A. N. Ivakin and J.-P. Sessarego, "High frequency broad band scattering from water-saturated granular sediments: Scaling effects," *J. Acoust. Soc. Am.*, vol. **122**, no. 5, pp. EL165–EL171, 2007.

[11] D. R. Jackson and M. D. Richardson, *High-Frequency Seafloor Acoustics*, ser. Monograph series in underwater acoustics. New York: Springer, 2007, ch. 2, 7, 14.

[12] H. Medwin and C. S. Clay, *Fundamentals of Acoustical Oceanography*. Boston: Academic Press, 1998, ch. 9.

[13] X. Lurton, *An Introduction to Underwater Acoustics: Principles and Applications*. Chichester, UK: Praxis Publishing, 2002, ch. 3.

[14] N. P. Chotiros, "Non-Rayleigh distributions in underwater acoustic reverberation in a patchy environment," *IEEE J. Oceanic Eng.*, vol. **35**, no. 2, pp. 236–241, 2010.

[15] M. Schrope, "Oil spill: Deep wounds," *Nature*, vol. **472**, no. 7342, pp. 152–154, 2011.

[16] S. A. Socolofsky, E. E. Adams, and C. R. Sherwood, "Formation dynamics of subsurface hydrocarbon intrunsions following the Deepwater Horizon blowout," *Geoph. Res. Lett.*, vol. **38**, no. 9, 2011.

[17] M. L. Ravalec, B. Noetinger, and L. Y. Hu, "The FFT moving average (FFT-MA) generator: An efficient numerical method for generating and conditioning Gaussian simulations," *Math. Geol.*, vol. **32**, no. 6, pp. 701–723, 2000.

[18] R. M. Gray, *Toeplitz and Circulant Matrices: A Review*. Found.Trends. Comm. Inf. Theory, 2006, vol. **2**, pp. 155–239.

[19] P. M. Morse and K. U. Ingard, *Theoretical Acoustics*, ser. International Series in Pure and Apllied Physics. New York: McGraw-Hill, 1968, ch. 8.

[20] V. Murino and A. Trucco, "Three-dimensional image generation and processing in underwater acoustic vision," *Proceedings of the IEEE*, vol. **88**, no. 12, pp. 1903–1984, 2000.

[21] L. A. Chernov, *Wave Propagation in a Random Medium*. New York: McGraw-Hill, 1960, ch. 4.

[22] V. Murino and A. Trucco, "Underwater 3D imaging by FFT dynamic focusing beamforming," in *Proceedings ICIP-94, IEEE International Conference*, vol. 1, Austin, TX, 1994, pp. 890–894.

[23] S. Dosso, P. Nielsen, and M. Wilmut, "Data error covariance in matched-field geoacoustic inversion," *J. Acoust. Soc. Am.*, vol. **119**, no. 1, pp. 208–219, 2006.

[24] R. M. Gray, "On the asymptotic eigenvalue distribution of Toeplitz matrices," *IEEE Trans. Inf. Theory*, vol. **18**, no. 6, pp. 725–730, 1972.

[25] R. Menon, P. Gerstoft, and W. S. Hodgkiss, "Asymptotic eigenvalue density of noise covariance matrices," *IEEE Trans. Signal Process.*, vol. **60**, no. 7, pp. 3415–3424, 2012.

[26] G. Wendelboe, H. Dahl, E. Maillard, and L. Bjorno, "Towards a fully calibrated multibeam echosounder," in *Proceedings of Meetings on Acoustics*, vol. 17, Edinburgh, UK, 2012, pp. 1836–1843.

[27] P. De Gennes and C. Taupin, "Microemulsions and the flexibility of oil/water interfaces," *J. Phys. Chem.*, vol. **86**, no. 13, pp. 2294–2304, 1982.

[28] P. Goovaerts, *Geostatistics for Natural Resources Evaluation*. New York: Oxford University Press, 1997, ch. 4.2.